Temperature dependence of internal friction in enzyme reactions

Anna Á. Rauscher,* Zoltán Simon,*,‡ Gergely J. Szöllősi,† László Gráf,* Imre Derényi,† and Andras Malnasi-Csizmadia*,1

*Department of Biochemistry and †Department of Biological Physics, Eötvös Loránd University, Budapest, Hungary; and ‡Delta Informatika, Inc., Budapest, Hungary

ABSTRACT   Our aim was to elucidate the physical background of internal friction of enzyme reactions by investigating the temperature dependence of internal viscosity. By rapid transient kinetic methods, we directly measured the rate constant of trypsin 4 activation, which is an interdomain conformational rearrangement, as a function of temperature and solvent viscosity. We found that the apparent internal viscosity shows an Arrhenius-like temperature dependence, which can be characterized by the activation energy of internal friction. Glycine and alanine mutations were introduced at a single position of the hinge of the interdomain region to evaluate how the flexibility of the hinge affects internal friction. We found that the apparent activation energies of the conformational change and the internal friction are interconvertible parameters depending on the protein flexibility. The more flexible a protein was, the greater proportion of the total activation energy of the reaction was observed as the apparent activation energy of internal friction. Based on the coupling of the internal and external movements of the protein during its conformational change, we constructed a model that quantitatively relates activation energy, internal friction, and protein flexibility.—Rauscher, A. Á., Simon, Z., Szöllősi, G. J., Gráf, L., Derényi, I., Malnasi-Csizmadia, A. Temperature dependence of internal friction in enzyme reactions. *FASEB J*. 25, 2804–2813 (2011). www.fasebj.org

ONE OF THE FUNDAMENTAL questions concerning the mechanisms of enzymatic reactions is how the dynamical properties of an enzyme affect the rate constants of its reaction steps. The conformational changes of a complex molecule in an aqueous medium are governed by frequent energy and momentum exchange (friction) between the atoms of the molecule and the surrounding medium, as a consequence of their perpetual collisions. Kramers (1, 2) has shown that in the overdamped regime (valid for most conformational changes) the rate of a transition over an energy barrier is inversely proportional to the coefficient of friction. Enzymes are large and complex molecules, and their reactions are influenced by not only external but also

internal friction, which has been pointed out in a seminal publication by Ansari *et al.* (3). Significant internal friction occurs during folding/unfolding reactions of proteins and enzymatic reactions coupled with conformational changes. Despite the intensive work on internal friction (4–8), no direct experimental approach has been developed to elucidate the physical origin of internal friction of an enzymatic reaction under native conditions. Here we present a systematic study of the temperature dependence of the internal friction of an enzymatic process, shedding light on its energetic background.

The effects of protein and solvent dynamics on enzymatic reactions are revealed by the temperature and viscosity dependence of the rate constants. By considering the coefficient of friction of an enzyme during its transition as a linear combination of two distinct coefficients characterizing external and internal friction, Ansari *et al.* (3, 4) have generalized the well-known Kramers formula for the rate constant:

$$k(T,\eta) = \frac{A}{\sigma + \eta} \exp\left(-\frac{\Delta E_a}{k_B T}\right) \qquad (1)$$

where A is a temperature- and viscosity-independent constant, ΔE_a is the activation energy, k_B is the Boltzmann constant, and T is the absolute temperature. The two sources of friction are the viscosity of the solvent η and a parameter, σ, which characterizes the protein and has the dimension of viscosity. This latter parameter is proportional to the magnitude of the internal friction of the protein and will be referred to as the "apparent internal viscosity." It is an intrinsic property of the protein and is specific to a certain conformational transition. The viscosity dependences of the rate constants for several reactions of proteins have been investigated to determine the values of σ at certain temperatures, *e.g.*, ligand binding of myoglobin (4), the folding of spectrin domains (6), cytochrome *c* (8), IgG binding domain of protein L (9), and Trp cage (10).

Recently, the σ values of trypsin activation reactions have also been determined at a single constant temperature (293 K; ref. 11). This reaction is accompanied by a large conformational rotation of a subdomain around a few interdomain hinges. Numerous hinge mutants of trypsin have demonstrated that the rate constant of the conformational change strongly depends on the bulkiness and the rotational freedom of the amino acids that form the hinges. Nevertheless, the physical basis of internal friction remains elusive. Our goal is to shed light on the energetic background of internal friction by determining the temperature dependence of the σ parameter of the conformational change that occurs on trypsin activation. Furthermore, by comparing two hinge mutants, we also investigate how internal friction is related to the flexibility of the hinge.

Trypsin activation is an enzymatic process when the inactive zymogen transforms to the active form of trypsin (**Fig. 1**). *In vitro*, a similar single-step reaction can be initiated by a rapid jump in pH (12–14). At high pH, the active trypsin acquires the zymogen conformation, which is transformed to the active form on pH reduction. The reaction can be followed by the change of the intrinsic tryptophan fluorescence in a stopped-flow apparatus (11, 15). The zymogen and the active forms are stable conformations of trypsinogen and trypsin, respectively, and their atomic crystal structures are available (1TGN, 2PTN). The activation process occurs naturally when the N-terminal peptide of the zymogen form of trypsin is proteolytically cleaved by another protease. Trypsin activation is a domain rearrangement that occurs by the rotation of a separate domain called activation domain around 5 glycine hinges (residues 19, 142, 184, 193, 216; refs. 16, 17). The role of these glycines in the activation process and the proteolytic activity of trypsin were deeply investigated recently (17). Except for Gly193, the alanine

mutations of these glycines dramatically reduce the proteolytic activity of trypsin. Although Gly193 is located next to the active site, its alanine mutation causes very little change in all enzymatic steps of the proteolysis (17). Nevertheless, Gly193 plays a major role as a hinge in the activation process, because a large rotation of the backbone occurs at this position: the values for the peptide backbone dihedral angles at Gly193 are $\Phi = 148.78°$ and $\Psi = 18.18°$ in trypsinogen (1TGN), while in trypsin these values change to $\Phi = 105.48°$ and $\Psi = 19.18°$ (2PTN). Recently, we showed that activation slowed by replacing this glycine with alanine or bulkier sidechains (11); however, the conformation of trypsin is affected slightly and only locally at this sidechain as it is indicated by the small activity change and also confirmed by molecular modeling (18). We also found that the apparent activation energies of the activation of these mutants did not change, but the slower processes caused by the mutations with bulky sidechains at position 193 were the consequences of the increased apparent internal viscosities (11). Trypsin activation is thus an ideal model process for the investigation of the internal friction during enzymatic conformational changes, because it is a well-defined single-step reaction between two conformers manifested by the rotation of a distinct domain around a few glycine hinges, and the mutations of one of the hinges (Gly193) cause highly specific changes in the apparent internal viscosity parameter σ of activation without affecting the structural and activity properties of the protein.

In this study, the temperature dependence and viscosity dependence of the conformational change on activation of mutants of human trypsin 4 (HuTry4), a well-characterized trypsin form (Protein Data Bank ID: 1H4W; ref. 19), are presented. In particular, the activation processes of two constructs in which either a glycine or an alanine is placed at the 193 hinge position (193G and 193A constructs, respectively) are compared. We performed systematic measurements on the 193G and 193A constructs of HuTry4 aimed at measuring the rate constant as a function of temperature and viscosity. The joint control of these two variables has enabled us to determine the temperature dependence of the apparent internal viscosity. From these data, we found that the internal viscosity depends exponentially on the reciprocal of temperature. We have also found that the apparent internal viscosity and its temperature dependence are strongly affected by the Gly-Ala replacement.
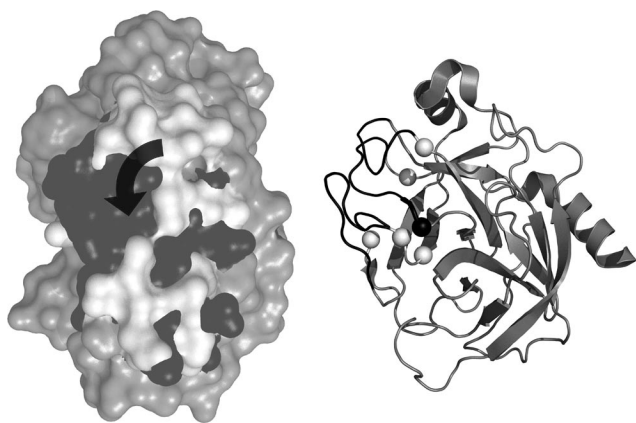
Figure 1. Overlaid atomic structures of the zymogen and active forms of trypsin. Left: during trypsinogen activation, the activation domain changes its conformation from the zymogen (white, 1TGN) to the active (dark gray, 2PTN) structure. The rest of the molecule (light gray) does not change its conformation. Right: trypsin active structure. Activation domain (black) consists of 4 loops that rotate around 5 glycine hinges (white and black spheres). Position 193 is shown in black.

MATERIALS AND METHODS

The rate constants of the conformation change of HuTry4 193A and 193G mutants triggered by pH jump from pH 11 to pH 8 were measured in solutions of different temperature and maltose concentrations. The pH jump was produced in the following way: a low buffer capacity solution containing the enzyme at pH 11 was rapidly mixed with a solution of high

buffer capacity at lower pH so that the mixture had the correct pH value of 8.

Determining the viscosity of solutions

The viscosity of the following solutions was measured: 0.1 M–1 M maltose and 50 mM HEPES with or without 150 mM NaCl in water. Details of the measurement can be found in Supplemental Material. An empirical equation was constructed to describe the viscosity of the solutions as a function of temperature and maltose concentration:

$$\eta(T,[maltose]) = (A[maltose]^3 + B[maltose]^2 + C[maltose] + D)\exp\left(\frac{E_\eta}{k_B(T - T_0)}\right) \quad (2)$$

where the viscosity η is a Vogel-Tamman-Fulcher (VTF)-like function (20) of temperature T and a polynomial function of maltose concentration, [maltose]. The viscosity of each solution was calculated from the fitted parameters found in **Table 1**.

Expression of enzyme, preparation, and mutation

The HuTry4 193A and 193G mutants were prepared as described by Toth and colleagues (11, 21).

Transient kinetic measurements

Measurements were carried out in the 275–311 K temperature range with 3 K increments in solutions of different maltose concentrations. A stopped-flow apparatus (SF-2004; KinTek Corp., Austin, TX) was used to record transients.

A CABS solution containing 2 mM CABS, 5 mM $CaCl_2$, 0–1 M maltose, and the enzyme at pH 10.5 was rapidly mixed in a 1:1 ratio with a HEPES solution containing ~50 mM HEPES, 5 mM $CaCl_2$, and the same amount of maltose as in the CABS solution. All reagents were produced by Sigma-Aldrich (St. Louis, MO, USA). The enzyme concentration after mixing was 1 μM, and the pH changed to pH 8.

By carefully choosing the cosolvents, we kept other variables constant as much as possible. HEPES and CABS were chosen as buffers because their pK values do not vary significantly with temperature. The HEPES concentration was slightly modified depending on the measuring temperature to keep the ionic strength constant; the exact concentration of HEPES in the premix solution was 65 mM at 275–287 K, 52 mM at 290–299 K, and 42 mM at 302–311 K. An online recipe calculator for thermodynamically correct buffers (http://www.liv.ac.uk/buffers/buffercalc.html) was used to set the ionic strength of the solutions. Maltose concentration in the

solutions varied from 0 to 1 M with 0.1 M increments. Maltose was chosen as a viscogen because it modifies the dielectric constant of the solution less compared with other widely used viscogens, such as glycerol.

The pH jump due to mixing triggered the conformation change of the enzyme, which resulted in an increase in fluorescence intensity. For measurement of this fluorescence change, the tryptophan residues were excited by 297 ± 2 nm wavelength light using a super quiet Hg-Xe lamp (150 W; Hamatsu Photonics UK Ltd., Welwyn Garden City, UK), and the emitted light was detected through a 340-nm interference filter (Comar Instruments, Cambridge, UK) by a PMT set to 700 V. In most cases, the fluorescence intensity change followed a single exponential that corresponds to a single-step reaction. In a few occasions, a small (<15% of the total intensity) and slow second phase also appeared, the mechanism of which remained unsolved.

Fitting procedure, visualization

All measurements were repeated 5–7 times, and exponential functions were fitted to the averaged transient traces by the KinTek software (KinTek Corp., Austin, TX, USA). The observed rate constants *vs.* temperature and viscosity data were fitted by the gnuplot software, using the least-squares method. Eq. 8 was transformed to the form

$$k(T,\eta) = \frac{A_{300}}{\eta + \sigma_{300}\exp\left(\frac{\Delta E_\sigma}{k_B}\left(\frac{1}{T} - \frac{1}{300\ K}\right)\right)}\exp$$
$$\left(-\frac{\Delta E_{SUM} - \Delta E_\sigma}{k_B}\left(\frac{1}{T} - \frac{1}{300\ K}\right)\right) \quad (3)$$

and then fitted to the data points. The transformation was necessary to optimize the fitting for data around 300 K and to minimize the correlation of the energy values ΔE_σ and ΔE_a.

The original parameters of Eq. 8 can be calculated from the fitting parameters:

$$A = A_{300}\exp\left(\frac{\Delta E_{SUM} - \Delta E_\sigma}{k_B 300\ K}\right) \quad (4)$$

$$\sigma_0 = \sigma_{300}\exp\left(-\frac{\Delta E_\sigma}{k_B 300\ K}\right) \quad (5)$$

$$\Delta E_a = \Delta E_{SUM} - \Delta E_\sigma \quad (6)$$

RESULTS

Temperature- and viscosity-dependent activation of HuTry4

The rate constants of the activation of 193G and 193A HuTry4 constructs were determined at different temperatures and viscosities. Reactions were initiated by pH jump from pH 11 to 8, and the reactions were followed by the intrinsic tryptophan fluorescence change in a stopped-flow apparatus. The pH jump induced a conformational rearrangement, which resulted in forming the active trypsin from the zymogen conformation. On the reaction of both constructs, a 20% fluorescence intensity increase was detected (**Fig. 2A**). The measurements were carried out at 13 different temperatures between 275 and 311 K and at 11 different concentra-

TABLE 1. *Fitting parameters for Eq. 2: surface fitted to the viscosity of solutions*

Fitting parameter	Solution	
	50 mM HEPES; 0–1 mM maltose	50 mM HEPES; 150 mM NaCl; 0–1 mM maltose
A (cP·M^{-3})	0.133 ± 0.054	0.174 ± 0.057
B (cP·M^{-2})	0.0155 ± 0.065	−0.0722 ± 0.045
C (cP·M^{-1})	0.107 ± 0.038	0.105 ± 0.035
D (cP)	0.107 ± 0.027	0.0686 ± 0.020
E_η (k·mol^{-1})	1.23 ± 0.28	1.70 ± 0.37
T_0 (K)	225 ± 7	215 ± 8

Values are means ± SE.
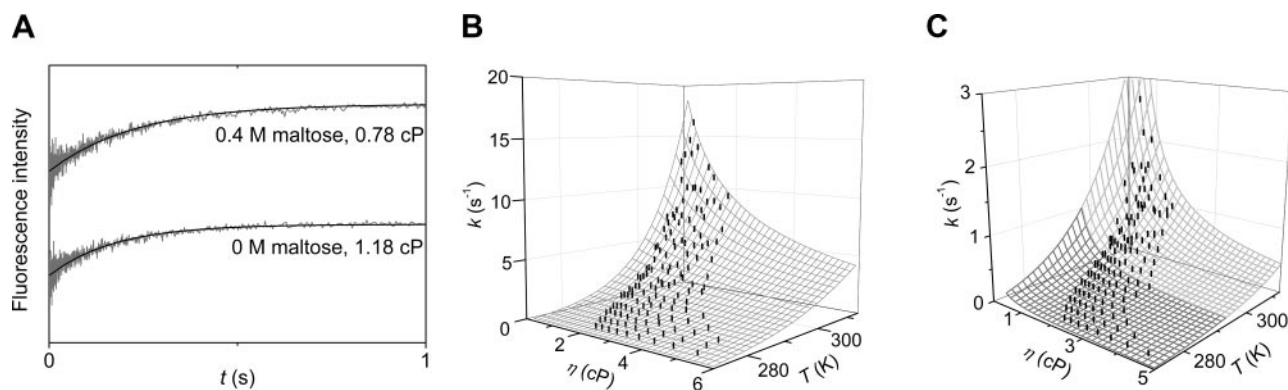
Figure 2. Temperature and viscosity dependence of the activation step of 193G and 193A constructs. *A*) Typical stopped-flow records of activation for 193G in the absence and presence of added viscogen at 299 K. Time courses of the reactions were fitted with single exponentials (solid black traces). *B, C*) Measured rate constants were plotted against viscosity and temperature for 193G (*B*) and for 193A (*C*). Best fits by Eq. 8 are represented by the surface grids. In the case of 193A, separate fitting procedures were carried out below (dark gray surface grid) and above (light gray surface grid) 293 K.

tions of maltose (which was used as viscogen) between 0 and 1 M, corresponding to a range of solvent viscosities between ~0.6 and 6 cP in water-based buffers (Fig. 2*B*, *C*). The viscosities of the buffers were determined by capillary viscometer at each temperature at >80 points (8 different temperatures, 11 different concentrations of maltose; see Materials and Methods and Supplemental Material). The permittivity of the solutions never changed >10% compared with water. We also carefully chose the buffer condition at each temperature such that the ionic strength of the solution did not change >5%.

The activation reaction of 193A was typically an order of magnitude slower than that of 193G under the same conditions. The reaction records were single phases, indicating single-step conformational rearrangements (Fig. 2*A*). The increased viscosity highly decreased the rate constants of the reactions for both constructs; however, the amplitudes did not change substantially. The reactions were also temperature sensitive.

Internal viscosity has Arrhenius-like temperature dependence

For both constructs, the reactions were measured at >130 different viscosity and temperature conditions (Fig. 2*B*, *C*). The rate constants were determined by fitting single exponentials to the stopped-flow records (Fig. 2*A*). By plotting the reciprocal of the isothermal rate constants against solvent viscosity, we could test the validity of Eq. 1 over the applied temperature and viscosity range. We found that the equation holds, as the viscosity dependence of the reciprocal of the rate constants (reaction relaxation times) is approximately linear for both constructs (**Fig. 3*A***). Thus, Eq. 1 was applied to determine the internal viscosity σ at constant temperatures.

This σ can be plotted against temperature (Fig. 3*B*): the plots for 193A and 193G are nonlinear over the whole temperature range. Below 293 K, the values and the temperature dependence of the internal viscosity

for the 193A construct are markedly different from those of the 193G. Intriguingly, above 293 K both the internal viscosity and its temperature dependence are
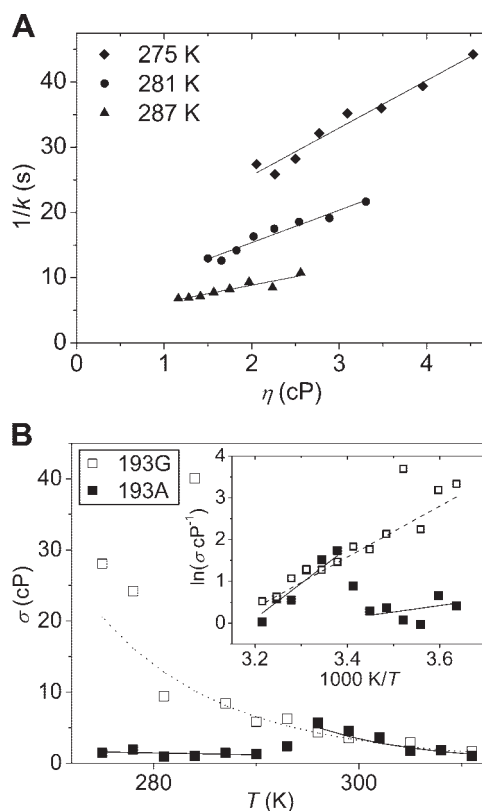
Figure 3. Internal viscosity calculated for every temperature from the linear viscosity dependence of the relaxation times. *A*) Typical viscosity dependence of the relaxation time (1/*k*) of the 193A construct. Internal viscosity σ can be determined from the intercept of the fitted line with the horizontal axis at every temperature. *B*) Internal viscosity σ is plotted against temperature. Dotted (193G) and solid (193A) lines represent σ as a function of temperature calculated from the fitted surface shown in Fig. 2*B*, *C*. Inset: natural logarithm of internal viscosity plotted against the reciprocal of temperature.

practically identical for both constructs. When the logarithm of the internal viscosity is plotted against the reciprocal of the absolute temperature (Fig. 3B, inset), the functions show linear relations in all three cases (193G on the entire temperature range; 193A below 293 K; and 193A above 293 K). Thus, we applied an Arrhenius type equation to fit the data points:

$$\sigma(T) = \sigma_0 \exp\left(\frac{\Delta E_\sigma}{k_B T}\right) \qquad (7)$$

where the characteristic energy ΔE_σ (the activation energy of internal friction) describes the temperature dependence of the internal viscosity, and σ_0 is a temperature-independent prefactor. Plugging Eq. 7 into Eq. 1 results in:

$$k(T,\eta) = \frac{A}{\eta + \sigma_0 \exp\left(\frac{\Delta E_\sigma}{k_B T}\right)} \exp\left(-\frac{\Delta E_a}{k_B T}\right) \qquad (8)$$

The same functional form for the viscosity and temperature dependence of the folding rate of cytochrome c was also observed by Pabit *et al.* (8) and for the folding/unfolding rates of Trp cage by Qiu and Hagen (10).

Dynamic phase transition of the 193A mutant at 293 K

We have found that ΔE_σ of 193A below 293 K is much smaller than that of 193A above 293 K and 193G (**Table 2**). In brief, two phases in the temperature dependence of the internal viscosity can be distinguished for the 193A mutant: above 293 K, it follows an exponential trend similar to the 193G mutant, but below 293 K, it shows a markedly different (almost constant) tendency.

Rate constant as a function of viscosity and temperature

Instead of the above described 2-step fitting procedure (first fitting a linear equation to the isothermal rate constants *vs.* viscosity; then fitting an Arrhenius-like exponential to the σ *vs.* T data) we can use Eq. 8 for fitting a surface to our measurement points (Fig. 2B, C and Table 2) in the (T, η) parameter space for each of the three cases (193G on the entire temperature range;

193A below 293 K; and 193A above 293 K). The fitted parameters show that the activation energy of the reaction is similar for 193G and 193A above 293 K, whereas it is much higher for 193A at lower temperatures (Table 2).

Measurements at higher ionic strength

The experiments described above were carried out in low-ionic-strength buffer systems ($I = 32 \pm 1$ mM). We also tested the viscosity dependence of the reaction rate constants of both mutants at a slightly higher ionic strength ($I = 187 \pm 3$ mM) in a smaller viscosity range (data not shown). Interestingly, we found that the internal viscosities and the activation energies of both the 193A and 193G mutants in the whole range of the studied temperature were similar to that of 193A at low ionic strength below 293 K, and no phase transition was detected (Table 2).

Arrhenius plots

As we have found earlier (11), the classical Arrhenius plots of 193G and 193A determined in a buffer without added viscogen are linear and parallel. The phase transition found in the temperature dependence of σ is not visible in the Arrhenius plot (**Fig. 4**). The reason for this is that the change of the temperature dependence of the internal viscosity at the critical temperature is largely compensated by the change of the activation energy, such that $\Delta E_\sigma + \Delta E_a$ remains almost the same. The implications of this phenomenon are discussed below.

DISCUSSION

Our aim was to unveil the physical origin of the apparent internal viscosity parameter σ of an enzymatic reaction accompanied by a large conformational change at native temperature and viscosity ranges. We wanted to learn about the energetic aspects of this internal viscosity by separating it from the external viscosity and determining its temperature dependence. For the object of our investigation, we chose the activation of trypsin mutants,

TABLE 2. *Parameters of the fitted surface in the (T, η) parameter space for Eq. 8*

Parameter	193G, $I = 32$ mM	193A below 293 K, $I = 32$ mM	193A above 293 K, $I = 32$ mM	193G, $I = 187$ mM	193A, $I = 187$ mM
Fitting parameter					
ΔE_σ (kJ·mol^{-1})	43.8 ± 11.5	16.1 ± 17.8	77.2 ± 30.1	0 ± 10.5	2.4 ± 6.8
ΔE_{SUM} (kJ·mol^{-1})	77.1 ± 2.7	67.7 ± 10.9	97.2 ± 10.0	70.0 ± 2.8	60.4 ± 3.6
σ_{300} (cP at 300 K)	3.97 ± 0.83	0.940 ± 0.420	3.62 ± 1.22	3.48 ± 1.96	1.17 ± 0.24
A_{300} (cP·s^{-1})	3.11 ± 0.15	-0.099 ± 0.18	0.85 ± 0.25	3.19 ± 0.44	0.30 ± 0.11
Calculated value					
ΔE_a (kJ·mol^{-1})	33.3	51.6	20.0	73.7	58.0
A (cP·s^{-1})	1.4×10^7	8.64×10^8	7.07×10^3	1.62×10^{14}	1.69×10^{10}

Values are means ± SE.
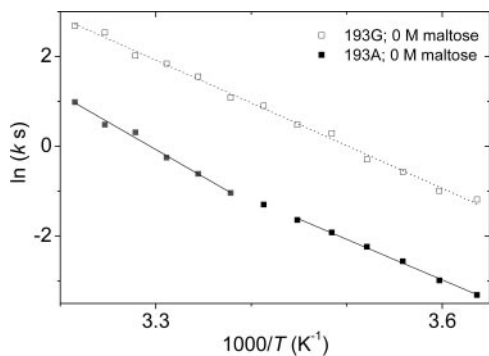
Figure 4. Arrhenius plots are linear and parallel for both constructs. Logarithm of reaction rate constant is plotted against the reciprocal of the absolute temperature on these Arrhenius plots of the activation of 193G and 193A in water-based buffer system (0 M maltose). Slope of the fitted line is proportional to the activation energy of the reaction.

which is a well-characterized viscosity- and temperature-dependent domain movement. We found that the reciprocal of the rate constant (*i.e.*, the relaxation time) of the domain movement of trypsin depends linearly on solvent viscosity with a nonzero limit at zero viscosity (11). This indicates that domain movements are also restricted by internal friction, characterized by σ. To unravel the physical background of σ, we determined its temperature dependence and found an Arrhenius-like relationship, implying that internal friction is associated with microscopic barrier-crossing events, in analogy with the mechanism underlying the viscosity of liquids (22).

Recent experimental and theoretical approaches for the viscosity dependence of rate constants

Several theoretical models have been suggested to explain the restriction of reactions by internal friction. However, most of these models reflect to protein-folding processes, and neither theoretical nor experimental investigations have been done to explore σ in native movements of protein domains. Protein folding takes place in a substantially broader configurational space than the reactions of native proteins. The theories that were developed for protein folding nevertheless may provide a good starting point for the investigation of extended conformational changes of native proteins, because the complex multicoordinate folding reactions are often simplified to processes containing only a few reaction coordinates.

Classic studies indicated that the kinetics of myoglobin ligand binding is slowed by internal friction (3, 23). Recently, Wensley *et al.* (6) characterized the folding process of spectrin domain also on the same experimental and theoretical basis: by increasing the concentration of some viscogenic cosolvent, they observed a linear viscosity dependence of the relaxation time of the reaction, with a nonzero limit at zero viscosity. Based on their results, they suggested that internal friction is related to energy landscape roughness. A more direct confirmation of this relationship would

require the determination of not only the viscosity dependence but also the temperature dependence of the reaction. This was missing in the original study.

Both the temperature and viscosity dependence were measured for cytochrome *c* folding (8) and for Trp cage folding/unfolding (10) by Hagen and colleagues, who also found a linear viscosity dependence of the relaxation time. Moreover, the temperature dependence of both the viscosity dependent and independent terms could be well fitted by two Arrhenius-like functions, leading to Eq. 9:

$$k_f^{-1} = \tau_s + \tau_{\text{int}} = A_s \eta \exp\left(\frac{\Delta H_s}{k_B T}\right) + B_{\text{int}} \exp\left(\frac{\Delta E_{\text{int}}}{k_B T}\right)$$

(9)

which is a mathematically equivalent, rearranged form of Eq. 8 (with $\Delta H_s = \Delta E_a$, $\Delta E_{\text{int}} = \Delta E_a + \Delta E_\sigma$, $A_s = 1/A$, and $B_{\text{int}} = \sigma_0/A$). Based on this formula, they interpreted the relaxation time of folding/unfolding as the sum of the relaxation times of two separate, sequential events characterized by two activation energies, ΔH_s and ΔE_{int}. Folding/unfolding was thus suggested to be a 2-step process, consisting of a reorganization of solvent-exposed regions of the molecule, followed/preceded by a substantial conformational rearrangement within the compact interiors with little displacement of the surrounding solvent (24). This 2-step picture, however, seems to be in contradiction with the single-exponential nature of the observed time courses, which is the signature of single-step processes. For 2-step processes, a lag or a burst phase should always appear in their time courses. Nonetheless the results, as also emphasized by the researchers, indicate that the concept of a single reaction coordinate with a homogeneous friction is insufficient to describe the observed phenomena; thus a more complex model is required.

Based on the concept of two perpendicular reaction coordinates (25), Zwanzig (26) interpreted the weaker than inverse proportionality of the rate constants on solvent viscosity by assuming that only one of the reaction coordinates is affected by the viscosity of the external medium. Although the predicted power law dependence of the rate constants on the viscosity is difficult to distinguish from Eq. 8 in the viscosity range of our experiments, the theory by itself cannot be applied to our data, as the time course of the transition implied by this model also deviates significantly from a single exponential.

A model with elastically coupled, parallel reaction coordinates

Here we establish a model that reconciles all the experimental data and relates the internal viscosity parameter to the microscopic properties of the protein. This model considers two parallel reaction coordinates and simultaneously explains the exponential time course of the reaction; the Arrhenius-like temperature dependence of the internal viscosity σ; and the finding

that although ΔE_a and ΔE_σ can take substantially different values under different experimental conditions (*e.g.*, point mutations, temperatures), their sum varies much less.

Following the line of thought of Ansari *et al.* (3), it is natural to divide the reaction coordinate into two, where one coordinate (the internal reaction coordinate) represents those atomic displacements that occur primarily inside the protein and are responsible mainly for the internal friction, whereas the other coordinate (the external reaction coordinate) represents the atomic displacements contributing mainly to the relocation of the surrounding solvent molecules causing the external friction. As an example, when a protein domain slides along another one, the trajectories of the domain-domain and the domain-water interfaces can be considered as the internal and external reaction coordinates, respectively. The two reaction coordinates are coupled to each other, and the strength of the coupling can be characterized by an elastic spring constant, κ (**Fig. 5**). In the limit of rigid coupling, the distinction between the two reaction coordinates diminishes, and the description in terms of a single reaction coordinate is recovered.

Let us now consider a conformational transition over an energy barrier (of height ΔE_1) and, based on the seminal work of Frauenfelder and colleagues (27, 28), suppose that the energy landscape along the internal reaction coordinate x_{int} is not smooth but has an additional roughness (of height ΔE_2), as depicted in Fig. 5. The external reaction coordinate x_{ext}, on the other hand, which represents the protein's displacement with respect to the surrounding fluid medium (a viscous milieu), can simply be characterized by a flat energy landscape. The friction coefficients associated with the internal end external reaction coordinates are denoted by γ_{int} and γ_{ext}, respectively. If there is a significant elastic coupling between the two reaction coordinates (such that they never become appreciably separated), which is a reasonable assumption for most enzymatic conformational changes, then it is sufficient to keep track of only one of the reaction coordinates (which we choose to be the external one, x_{ext}, for convenience) to describe the transition. Consequently, the diffusive motion of the system along this external reaction coordinate will appear as if it occurred in an effective potential (E_{eff}) with some effective friction coefficient (γ_{eff}). For details, see the Appendix.

In case of stiff coupling (*i.e.*, when the two reaction coordinates are practically identical), the effective potential coincides with the energy surface of the internal
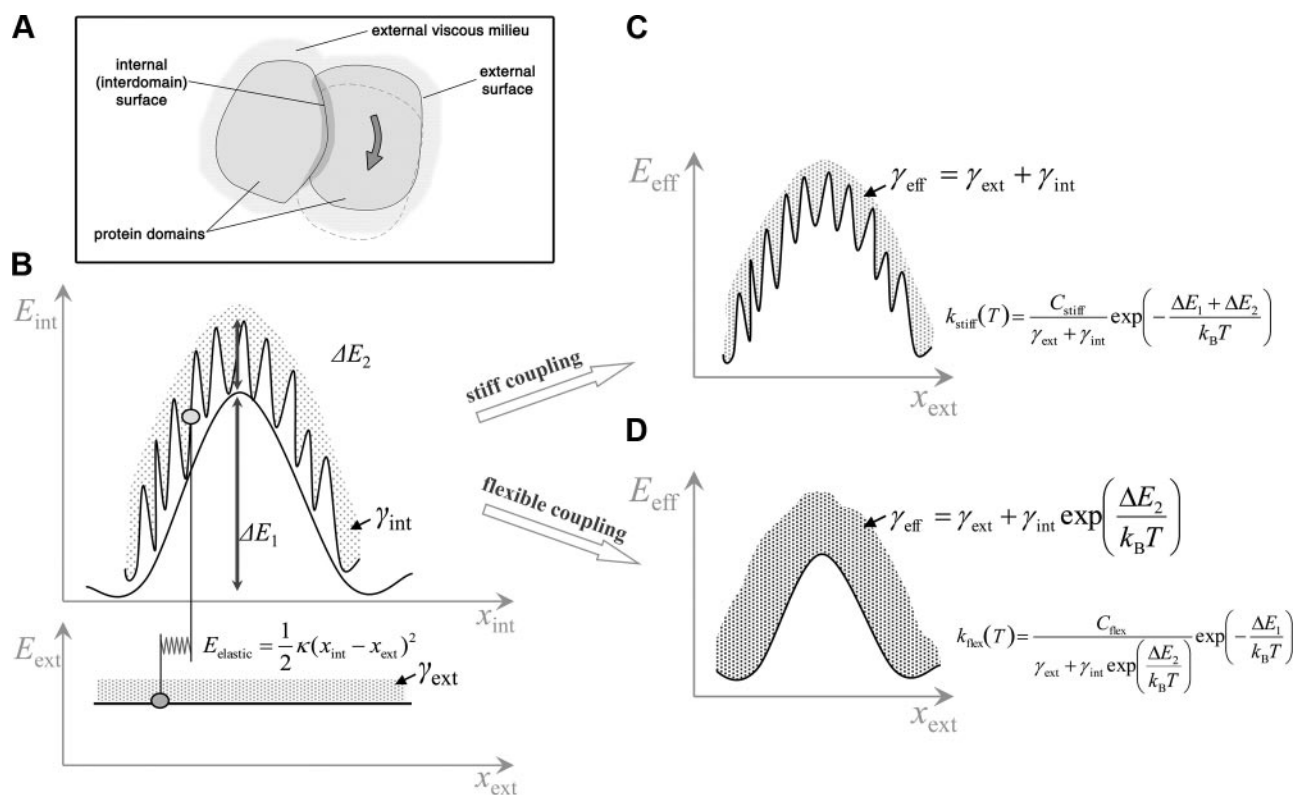
Figure 5. Apparent energy landscape is affected by protein flexibility. *A*) During a protein conformational change, relative movement between domain-domain and domain-water interfaces occurs. *B*) These movements can be described along two reaction coordinates coupled by an elastic component. Elastic component is represented by the bodies of the protein domains between the moving surfaces. Reactions on both coordinates are limited by internal and external friction (with coefficients γ_{int} and γ_{ext}, respectively). *C*) When the elastic component is rigid, the effective energy landscape experienced by the external reaction coordinate coincides with the energy surface of the internal movements, and the effective friction coefficient will be the sum of the internal and external coefficients. *D*) When the coupling is flexible, the roughness of the effective energy landscape is smoothed out, resulting in the increase of the effective friction coefficient by a factor of $\exp[\Delta E_2/(k_B T)]$ and the concomitant decrease of the effective activation energy barrier by ΔE_2.

potential (resulting in $\Delta E_{\text{eff}} = \Delta E_1 + \Delta E_2$), and the effective friction coefficient is the sum of the external and internal friction coefficients ($\gamma_{\text{eff}} = \gamma_{\text{ext}} + \gamma_{\text{int}}$). Thus, the rate constant of the transition will be

$$k_{\text{stiff}}(T) = \frac{C_{\text{stiff}}}{\gamma_{\text{ext}} + \gamma_{\text{int}}} \exp\left(-\frac{\Delta E_1 + \Delta E_2}{k_B T}\right) \quad (10)$$

where C_{stiff} is a constant prefactor.

If, however, the coupling is weaker [*i.e.*, $(\Delta E_2 / \kappa)^{1/2}$ becomes larger than the characteristic length scale of the roughness], then for the external reaction coordinate, the roughness of the internal energy landscape will be smeared into an increased apparent internal friction coefficient by about a factor of $\exp [\Delta E_2 / (k_B T)]$. This factor can be easily understood by recognizing that the apparent diffusion in a rough potential proceeds by random hopping over the energy barriers (of height ΔE_2) of the rough landscape at a rate proportional to $\exp [-\Delta E_2 / (k_B T)]$, and the apparent friction coefficient is inversely proportional to the apparent diffusion coefficient (6, 29, 30). Thus, the effective potential will be only the smooth part of the internal energy surface ($\Delta E_{\text{eff}} = \Delta E_1$); the effective friction coefficient will be the sum of the external and the increased apparent internal friction coefficients ($\gamma_{\text{eff}} = \gamma_{\text{ext}} + \gamma_{\text{int}} \exp [\Delta E_2 / (k_B T)]$); and the rate constant of the transition will become

$$k_{\text{flex}}(T) = \frac{C_{\text{flex}}}{\gamma_{\text{ext}} + \gamma_{\text{int}} \exp\left(\dfrac{\Delta E_2}{k_B T}\right)} \exp\left(-\frac{\Delta E_1}{k_B T}\right)$$

$$(11)$$

where C_{flex} is another prefactor.

In general, if the energy landscape characterizing the internal reaction coordinate contains wells and barriers at various scales (27, 31, 32), then due to the flexibility of the protein, the undulations at short length scales will be experimentally observed as an increase of the apparent internal friction and a concomitant decrease of the apparent activation energy (see **Fig. 6**). Larger flexibility will smear wider (and usually higher) undulations into the apparent internal friction. The typical value of the critical length scale below which the

roughness is smeared out (for nanometer-sized domains with Young moduli of a few gigapascals, and for landscape roughness of the order of 10 kJ/mol) falls in the physically reasonable angstrom range.

Thus the exponential dependence of the apparent internal viscosity on the reciprocal of the temperature, as given in Eq. 7, during a conformational transition can be interpreted as the incorporation of the short-length-scale roughness of the internal reaction coordinate into the apparent internal friction by the factor $\exp [\Delta E_\sigma / (k_B T)]$. At the same time, the observed activation energy ΔE_a is smaller than its true value by ΔE_σ. It is thus the flexibility of the protein that determines what proportion of the undulations of the energy landscape is experienced as a contribution to the activation energy ΔE_a or to the internal friction (through ΔE_σ) but in such a way that the sum $\Delta E_a + \Delta E_\sigma$ remains constant.

This is exactly what we see for our trypsin mutants: the sum of $\Delta E_a + \Delta E_\sigma$ has a similar value in every temperature range of each mutant, and this value is also consistent with the activation energy calculated from the classical Arrhenius plots (in the absence of any viscogenic cosolvent). The functional form of the rate constant implied by our model is also mathematically equivalent to that established experimentally by Hagen and colleagues (8, 10), but our model has the advantage that it does not require a multiphasic time course of the reactions.

The 193G mutant, which has a more flexible hinge, showed a much stronger temperature dependence of the internal viscosity and consequently a higher ΔE_σ than the 193A at low temperatures. It seems that the rotational freedom of the hinge is strongly related to the ratio of ΔE_a and ΔE_σ. Furthermore, for the 193A mutant, we found a sudden decrease of ΔE_a and a similar amount of increase of ΔE_σ at 293 K. At this temperature, the low value of ΔE_σ jumps to the same value as that of 193G, indicating that a significant change (similar to a phase transition) must occur either in the flexibility of the protein or in the pathway of the transition but in such a way that the total height of the activation barrier ($\Delta E_a + \Delta E_\sigma$) remains largely intact. This intriguing effect succinctly demonstrates that in

Stiff coupling   Moderate flexibility   High flexibility
                  (*Ala* mutant)   (*Gly* mutant)
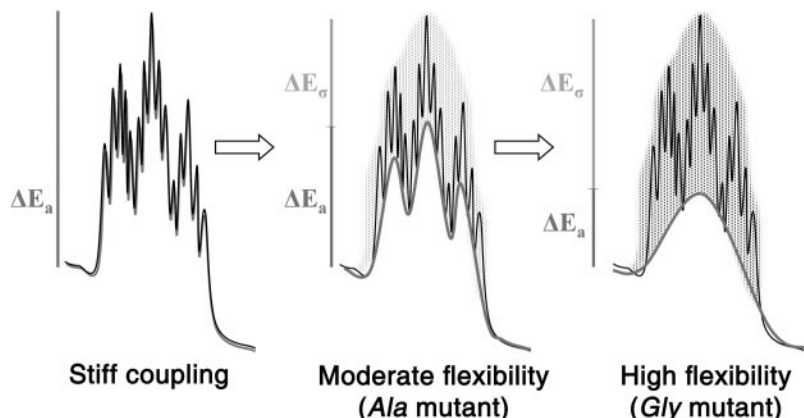
Figure 6. Schematic representation of the hierarchy of roughness of the energy landscape. Depending on the flexibility of the protein, different effective energy landscapes can be observed. Same energy landscape (black traces) results in different apparent energy barriers (gray traces, ΔE_a) depending on the degree of flexibility of the protein and the hierarchical levels of the roughness of the landscape. The remaining part of the total activation energy that is left out of the effective energy barrier appears as a contribution to the activation energy for internal diffusion (ΔE_σ). The sum of ΔE_a and ΔE_σ is constant, irrespective of flexibility.

the same protein the proportions of ΔE_a and ΔE_σ could change at specific conditions but without changing their sum. In other words, the comparison of the reaction parameters of 193G and 193A at low and high temperatures supports the idea that the domain flexibility influences the ratio of ΔE_a and ΔE_σ but without significantly affecting the slope of the classic Arrhenius plot (Fig. 4), which is related to the total activation energy of the reaction.

Further experimental confirmation of our model was provided by the results obtained in high ionic strength conditions. In high-salt buffer systems, the temperature dependence of the internal viscosity of both constructs became similar to that of the 193A mutant measured at low ionic strength below 293 K, while the sum of the two energy components remained unchanged. We may speculate that the temperature of the phase transition increased to a value above the studied temperature range as the ionic strength was increased.

In summary, we have provided evidence that the measurement of the temperature dependence of the apparent internal viscosity during the conformational change of a protein, using low concentrations of viscogenic cosolvents can detect dynamic phase transitions that would otherwise remain hidden in a classical Arrhenius plot; and provide information on the structure of the energy landscape along the reaction coordinate and the flexibility of the affected parts of the protein. This is because the observed energy profile depends on the protein flexibility. In case of high flexibility, the roughness of the energy landscape appears as internal friction rather than a component of the energy barrier for the reaction. We highlight that the sum of the measured activation energy of the reaction ΔE_a and the activation energy of the internal friction ΔE_σ is fixed for a specific enzymatic reaction but their individual values are subject to the flexibility of the protein. Thus the apparent internal friction and activation energy values are interrelated parameters and depend on protein flexibility. [FJ]

Appendix: effective energy landscape and friction coefficient for two elastically coupled reaction coordinates

To understand how the roughness of the energy landscape of a reaction coordinate x_{int} translates into either the common effective potential E_{eff} or the common effective friction coefficient γ_{eff} of two elastically coupled reaction coordinates, x_{ext} and x_{int}, let us consider the simplest scenario, when the energy landscape E_{ext} of the external coordinate x_{ext} is flat, and the energy landscape E_{int} of the internal coordinate x_{int} consists of

a periodic series of energy barriers of height ΔE and period length L (as illustrated in **Fig. 7**). The coupling is characterized by the spring constant κ, and the friction coefficients of the external and internal reaction coordinates are denoted by γ_{ext} and γ_{int}, respectively. To determine the effective friction coefficient of the coupled system, we apply two constant external forces, F_1 and F_2 to the two reaction coordinates and calculate their average speed (which is necessarily the same for both of them). The calculation can easily be done in two limiting cases.

When the coupling is very rigid ($\kappa L^2 \gg \Delta E$), *i.e.*, when the expansion of the spring to distance L requires much more energy than climbing an energy barrier, the two reaction coordinates can be considered as a single one with an effective friction coefficient $\gamma_{eff} = \gamma_{ext} + \gamma_{int}$ moving in the superposition of the two energy landscapes with barriers of height ΔE. Their average speed is thus:

$$v_{rigid} = \frac{F_1 + F_2}{(\gamma_{ext} + \gamma_{int})\, c \exp\left(\dfrac{\Delta E}{k_B T}\right)} \tag{12}$$

where c is a geometrical factor, and it is approximately $k_B T/(\pi \Delta E)$ for sinusoidal potentials (29, 30).

For a very flexible coupling ($\kappa L^2 \ll \Delta E$), the two coordinates will be separated far apart, and the elastic element will exert an essentially constant elastic force F_e on both of them (with opposite signs). Their speed can thus be written as:

$$v_{flex} = \frac{F_1 - F_e}{\gamma_{ext}} \tag{13}$$

$$v_{flex} = \frac{F_2 + F_e}{\gamma_{int}\, c \exp\left(\dfrac{\Delta E}{k_B T}\right)} \tag{14}$$
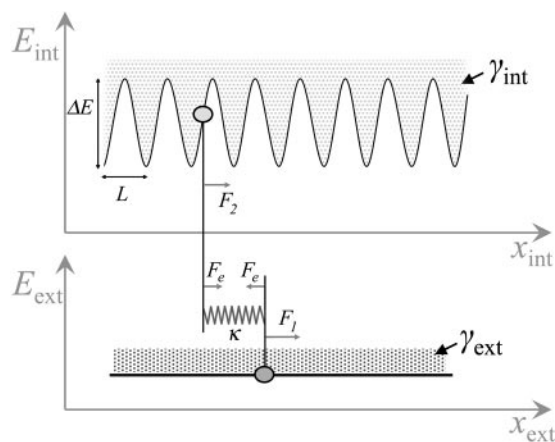
Figure 7. Simplified model system with two coupled reaction coordinates. Two reaction coordinates (x_{ext} and x_{int}) moving along two energy landscapes (E_{ext} and E_{int}) are coupled elastically (through a spring constant κ) and experience viscosities γ_{ext} and γ_{int}. To determine the effective friction coefficient of the coupled system, constant external forces (F_1 and F_2) are exerted on the two reaction coordinates.

The solution of this system of equations gives:

$$\nu_{\text{flex}} = \frac{F_1 + F_2}{\gamma_{\text{ext}} + \gamma_{\text{int}}\, c \exp\left(\dfrac{\Delta E}{k_B T}\right)} \qquad (15)$$

indicating that the barriers of the internal reaction coordinates is translated into the activation energy of the internal friction, resulting in an effective friction coefficient $\gamma_{\text{eff}} = \gamma_{\text{ext}} + \gamma_{\text{int}}\, c \exp[\Delta E/(k_B T)]$ for the coupled system.

REFERENCES

1. Kramers, H. A. (1940) Brownian motion in a field of force and the diffusion model of chemical reactions. *Physica* **7**, 284–304
2. Hänggi, P., Talkner, P., and Borkovec, M. (1990) Reaction-rate theory: fifty years after Kramers. *Rev. Mod. Phys.* **62**, 251–342
3. Ansari, A., Jones, C. M., Henry, E. R., Hofrichter, J., and Eaton, W. A. (1992) The role of solvent viscosity in the dynamics of protein conformational changes. *Science* **256**, 1796–1798
4. Ansari, A., Jones, C. M., Henry, E. R., Hofrichter, J., and Eaton, W. A. (1994) Conformational relaxation and ligand binding in myoglobin. *Biochemistry* **33**, 5128–5145
5. Suda, H. (2001) Origin of friction derived from rupture dynamics. *Langmuir* **17**, 6045
6. Wensley, B. G., Batey, S., Bone, F. A., Chan, Z. M., Tumelty, N. R., Steward, A., Kwa, L. G., Borgia, A., and Clarke, J. (2010) Experimental evidence for a frustrated energy landscape in a three-helix-bundle protein family. *Nature* **463**, 685–688
7. Neuweiler, H., Johnson, C. M., and Fersht, A. R. (2009) Direct observation of ultrafast folding and denatured state dynamics in single protein molecules. *Proc. Natl. Acad. Sci. U. S. A.* **106**, 18569–18574
8. Pabit, S. A., Roder, H., and Hagen, S. J. (2004) Internal friction controls the speed of protein folding from a compact configuration. *Biochemistry* **43**, 12532–12538
9. Plaxco, K. W., and Baker, D. (1998) Limited internal friction in the rate-limiting step of a two-state protein folding reaction. *Proc. Natl. Acad. Sci. U. S. A.* **95**, 13591–13596
10. Qiu, L., and Hagen, S. J. (2004) A limiting speed for protein folding at low solvent viscosity. *J. Am. Chem. Soc.* **126**, 3398–3399
11. Toth, J., Simon, Z., Medveczky, P., Gombos, L., Jelinek, B., Szilagyi, L., Graf, L., and Malnasi-Csizmadia, A. (2007) Site directed mutagenesis at position 193 of human trypsin 4 alters the rate of conformational change during activation: role of local internal viscosity in protein dynamics. *Proteins* **67**, 1119–1127
12. Fersht, A. R., and Renard, M. (1974) pH dependence of chymotrypsin catalysis. Appendix: substrate binding to dimeric alpha-chymotrypsin studied by x-ray diffraction and the equilibrium method. *Biochemistry* **13**, 1416–1426
13. Heremans, L., and Heremans, K. (1989) Raman spectroscopic study of the changes in secondary structure of chymotrypsin: effect of pH and pressure on the salt bridge. *Biochim. Biophys. Acta* **999**, 192–197
14. Stoesz, J. D., and Lumry, R. W. (1978) Refolding transition of alpha-chymotrypsin: pH and salt dependence. *Biochemistry* **17**, 3693–3699
15. Verheyden, G., Matrai, J., Volckaert, G., and Engelborghs, Y. (2004) A fluorescence stopped-flow kinetic study of the conformational activation of alpha-chymotrypsin and several mutants. *Protein Sci.* **13**, 2533–2540
16. Bode, W., Schwager, P., and Huber, R. (1978) The transition of bovine trypsinogen to a trypsin-like state upon strong ligand binding. The refined crystal structures of the bovine trypsinogen-pancreatic trypsin inhibitor complex and of its ternary complex with Ile-Val at 1.9 A resolution. *J. Mol. Biol.* **118**, 99–112
17. Gombos, L., Kardos, J., Patthy, A., Medveczky, P., Szilagyi, L., Malnasi-Csizmadia, A., and Graf, L. (2008) Probing conformational plasticity of the activation domain of trypsin: the role of glycine hinges. *Biochemistry* **47**, 1675–1684
18. Bobofchak, K. M., Pineda, A. O., Mathews, F. S., and Di Cera, E. (2005) Energetic and structural consequences of perturbing Gly-193 in the oxyanion hole of serine proteases. *J. Biol. Chem.* **280**, 25644–25650
19. Katona, G., Berglund, G. I., Hajdu, J., Graf, L., and Szilagyi, L. (2002) Crystal structure reveals basis for the inhibitor resistance of human brain trypsin. *J. Mol. Biol.* **315**, 1209–1218
20. Rampp, M., Buttersack, C., and Lüdemann, H.-D. (2000) c,T-Dependence of the viscosity and the self-diffusion coefficients in some aqueous carbohydrate solutions. *Carb. Res.* **328**, 561
21. Toth, J., Gombos, L., Simon, Z., Medveczky, P., Szilagyi, L., Graf, L., and Malnasi-Csizmadia, A. (2006) Thermodynamic analysis reveals structural rearrangement during the acylation step in human trypsin 4 on 4-methylumbelliferyl 4-guanidinobenzoate substrate analogue. *J. Biol. Chem.* **281**, 12596–12602
22. Viswanath, D. S., Ghosh, T. K., Prasad, D. H. L., Dutt, N. V. K., and Rani, K. Y. (2007). *Viscosity of Liquids*, Springer, Dordrecht, The Netherlands
23. Beece, D., Eisenstein, L., Frauenfelder, H., Good, D., Marden, M. C., Reinisch, L., Reynolds, A. H., Sorensen, L. B., and Yue, K. T. (1980) Solvent viscosity and protein dynamics. *Biochemistry* **19**, 5147–5157
24. Hagen, S. J. (2010) Solvent viscosity and friction in protein folding dynamics. *Curr. Protein Pept. Sci.* **11**, 385–395
25. Agmon, N., and Hopfield, J. J. (1982) Transient kinetics of chemical reactions with bounded diffusion perpendicular to the reaction coordinate: Intramolecular processes with slow conformational changes. *J. Chem. Phys.* **78**, 6947–6959
26. Zwanzig, R. (1992) Dynamical disorder: passage through a fluctuating bottleneck. *J. Chem. Phys.* **97**, 3587–3589
27. Frauenfelder, H., Sligar, S. G., and Wolynes, P. G. (1991) The energy landscapes and motions of proteins. *Science* **254**, 1598–1603
28. Ansari, A., Berendzen, J., Bowne, S. F., Frauenfelder, H., Iben, I. E., Sauke, T. B., Shyamsunder, E., and Young, R. D. (1985) Protein states and proteinquakes. *Proc. Natl. Acad. Sci. U. S. A.* **82**, 5000–5004
29. Festa, R., and d'Agliano, E. G. (1978) Diffusion coefficient for a Brownian particle in a periodic field of force: I. Large friction limit. *Phys. A Stat. Theor. Phys.* **90**, 229
30. Zwanzig, R. (1988) Diffusion in a rough potential. *Proc. Natl. Acad. Sci. U. S. A.* **85**, 2029–2030
31. Fenimore, P. W., Frauenfelder, H., McMahon, B. H., and Young, R. D. (2004) Bulk-solvent and hydration-shell fluctuations, similar to alpha- and beta-fluctuations in glasses, control protein motions and functions. *Proc. Natl. Acad. Sci. U. S. A.* **101**, 14408–14413
32. Nevo, R., Brumfeld, V., Kapon, R., Hinterdorfer, P., and Reich, Z. (2005) Direct measurement of protein energy landscape roughness. *EMBO Rep.* **6**, 482–486